Available online at www.sciencedirect.com

ScienceDirect

journal homepage: www.JournalofSurgicalResearch.com

Autofluorescence-Raman Spectroscopy for *Ex Vivo* Mapping Colorectal Liver Metastases and Liver Tissue

Christopher Corden, PhD,[a] *Radu Boitor, PhD,*[a] *Palminder Kaur Dusanjh, PhD,*[b] *Andrew Harwood, MSc,*[b] *Abhik Mukherjee, MBBS, PhD, FRCPath,*[b,c] *Dhanwant Gomez, MD, FRCS,*[d] *and Ioan Notingher, PhD*[a,*]

[a] *School of Physics and Astronomy, University of Nottingham, Nottingham, UK*
[b] *Histopathology Department, Nottingham University Hospitals NHS Trust, Queen's Medical Centre, Nottingham, UK*
[c] *School of Medicine, University of Nottingham, Nottingham, UK*
[d] *Department of Hepatobiliary and Pancreatic Surgery, Nottingham University Hospitals NHS Trust, Queen's Medical Centre, Nottingham, UK*

ARTICLE INFO

Article history:
Received 22 July 2022
Received in revised form
15 January 2023
Accepted 17 February 2023
Available online xxx

Keywords:
Auto-fluorescence
Colorectal liver metastases
Liver
Raman spectroscopy

ABSTRACT

Introduction: Identifying colorectal liver metastases (CRLM) during liver resection could assist in achieving clear surgical margins, which is an important prognostic variable for both disease-free and overall survival. The aim of this study was to investigate the effect of auto-fluorescence (AF) and Raman spectroscopy for *ex vivo* label-free discrimination of CRLMs from normal liver tissue. Secondary aims include exploring options for multimodal AF-Raman integration with respect to diagnosis accuracy and imaging speed on human liver tissue and CRLM.

Methods: Liver samples were obtained from patients undergoing liver surgery for CRLM who provided informed consent (15 patients were recruited). AF and Raman spectroscopy was performed on CRLM and normal liver tissue samples and then compared to histology.

Results: AF emission spectra demonstrated that the 671 nm and 775/785 nm excitation wavelengths provided the highest contrast, as normal liver tissue elicited on average around eight-fold higher AF intensity compared to CRLM. The use of the 785 nm wavelength had the advantage of enabling Raman spectroscopy measurements from CRLM regions, allowing discrimination of CRLM from regions of normal liver tissue eliciting unusual low AF intensity, preventing misclassification. Proof-of-concept experiments using small pieces of CRLM samples covered by large normal liver tissue demonstrated the feasibility of a dual-modality AF-Raman for detection of positive margins within few minutes.

* *Corresponding author*. School of Physics and Astronomy, University of Nottingham, University Park, NG7 2RD Nottingham, UK.
E-mail address: ioan.notingher@nottingham.ac.uk (I. Notingher).

https://doi.org/10.1016/j.jss.2023.02.014

Conclusions: AF imaging and Raman spectroscopy can discriminate CRLM from normal liver tissue in an *ex vivo* setting. These results suggest the potential for developing integrated multimodal AF-Raman imaging techniques for intraoperative assessment of surgical margins.

Introduction

Colorectal cancer is the third most commonly diagnosed cancer worldwide and approximately half of these patients will develop colorectal liver metastases (CRLM).[1,2] Liver resection remains the only potentially curative treatment for CRLM with 10-year survival rates of up to 23% been reported.[3] With the expansion of indications of liver resection in CRLM, the impact of achieving a clear margin in patients with heavy liver disease burden is not always possible. Nevertheless, studies have shown that a clear resection margin is associated with better overall survival.[4]

To date, there is no defined intraoperative technique to assess the resection margin following excision of liver tumours. Large studies have demonstrated that a clear resection margin significantly influences the survival outcome of patients with CRLM, irrespective of other co-founders.[5] This is more important in patients who have had downstaged chemotherapy, as these patients tend to have a heavier disease burden in the liver. In general, a liver parenchymal-sparing approach is adopted in such cases. Hence, achieving a clear margin is important and this could potentially translate into a lower incidence of disease recurrence, in particular at the margin site or other areas of the remnant liver. In CRLM, a longer disease-free survival leads to improved overall survival.[3,6] An intraoperative technique that could assist the hepatobiliary surgeon in determining the margin status could potentially influence survival outcomes. Following resection of the tumour, it is important to determine whether there is any remaining cancer tissue at the margin of the remnant liver. If there are remaining cancer cells, then a further margin can be excised; ablation of the liver margin or conversion to a more radical liver operation may be required.

A range of optical imaging techniques have been explored for intraoperative discrimination of tumour from surrounding normal tissue.[7] Fluorescence and Raman spectroscopy rely on interaction between light and endogenous tissue molecules and can provide high diagnostic specificity.[8,9] Furthermore, the combination of auto-fluorescence (AF) and Raman spectroscopy in a multimodal approach was shown to improve detection of positive margins for nonmelanoma skin cancer[10-12] and breast cancer,[13,14] with imaging times promising for its application in an intraoperative setting.

The liver has a range of intrinsic fluorophores, involved in metabolism [NAD(P)H, flavins, lipofuscins, retinoids, porphyrins, bilirubin, and lipids] or in structural architecture (aromatic amino acids, collagen, etc.), which are often altered in liver diseases and hence, can be used for diagnosis of liver cancers.[15] However, the first use of AF imaging for imaging surgical margins in liver surgery for primary liver tumours has recently been reported.[16] AF imaging based on 488 nm laser coupled to a confocal microscope allowed real-time differentiation of cancerous regions from noncancerous tissues in surgical specimens.[16] The study found fluorescence intensity values higher in noncancerous regions than in primary liver tumours: 104 (79.8-156) *versus* 74.9 (60.6-106), which were found to be statistically significant.

While Raman spectroscopy has been widely used for the discrimination of cancer from normal tissue for a range of organs,[17-20] the applications to malignancies in the liver have been limited because of the strong fluorescence background that saturates the Raman bands.[21] Time-gated Raman spectroscopy, a technique that uses lasers pulses and discriminated between Raman and fluorescence photons in the time domain, can reduce large background effects caused by fluorescence emission or ambient light.[22] However, this has not been applied to liver tissue.

The aim of this study was to investigate the effect of AF and Raman spectroscopy on *ex vivo* label-free discrimination of CRLMs from normal liver tissue. Secondary aims include exploring options for dual-modality AF-Raman integration with respect to diagnosis accuracy and imaging speed on human liver tissue and CRLM.

Patients and Methods

Patient recruitment, ethics approval, and tissue collection

All patients undergoing liver surgery for CRLM at Queen's Medical Centre, Nottingham University Hospitals NHS Trust, Nottingham, United Kingdom were considered for this study. Informed consent was obtained from all recruited patients. Liver resection was performed using the Cavi-Pulse Ultrasonic Surgical Aspirator. Intraoperative ultrasound was performed to confirm the findings of preoperative imaging and to assist in surgical planning. Type of surgical procedure was dependent on the resection of all macroscopic disease and achieving a clear resection margin, while preserving sufficient remnant liver.

Following surgery, samples of 1-2 cm in size were cut from regions of normal liver and CRLM from the excised liver specimens. This was performed by the Histopathology Department (PSD, AH, AM). All samples were then frozen and stored at −20°C immediately after cutting until the samples were thawed at room temperature and placed on a 1 mm thick quartz window for measurements. Tests on fresh and frozen porcine liver tissue (sourced from a local butcher) confirmed that freezing the liver tissue had no impact on the fluorescence and Raman spectra (Supplementary Information Fig. S2). During the study period, a total of 15 liver samples were collected and subsets were used for different part of the

study depending on the amount of sample and the collection date and stage in the project. None of the specimens had a background liver of cirrhosis.

The samples were given a study number from 1 to 15 and data were anonymized at collection from the Histopathology Department between the Hepatobiliary surgery team (D.G.) and the School of Physics research team (C.C., R.B., and I.N.), with patient identifying records stored separately in a file accessible only to the immediate Hepatobiliary team (D.G.). The data were stored on a secure NHS computer, on the hospital-based server on the Nottingham University Hospitals campus. This is firewall-protected with access limited by password only to the Hepatobiliary surgeon (D.G.) directly involved in the study. The information will be stored on a secure, password-protected, and fire-walled NHS computer. This information will not be available to anyone outside of the clinical team.

Ethical approval was granted by the Health Research Authority and Health and Care Research Wales and East-Midlands Leicester South Research Ethics Committee (reference 20/EM/0184).

Chemotherapy data

In these liver samples, nine of the 15 samples had preoperative systemic chemotherapy. Patients scheduled for preoperative systemic chemotherapy had 3-6 mo of neoadjuvant treatment. The regimens used were either Oxaliplatin based: two weekly FOLFOX [5-fluorouracil (FU) 400 mg/m^2 bolus and 2400 mg/m^2 over 46 h, Leucovorin and Oxaliplatin 85 mg/m^2] or three weekly CAPOX (Capecitabine 1000 mg/m^2 BD for 14 d and Oxaliplatin 130 mg/m^2).

However, in patients tested and found to be *RAS* wild-type, two weekly FOLFIRI (Irinotecan 180 mg/m^2, 5-FU 400 mg/m^2 bolus, and 2400 mg/m^2 over 46 h) was administered with concurrent Cetuximab (400 mg/m^2 cycle 1, then 250 mg/m^2 cycle 2 onward).

The response to neoadjuvant therapy was assessed after 3-6 mo of therapy by computed tomography scan and repeat magnetic resonance imaging of the liver if required. Patients were then rediscussed at the multi-disciplinary team and considered for surgery based on absence of new disease, tumour response, and extent of disease. Patients deemed to have resectable disease were scheduled for a liver resection, 4-6 wk after their last cycle of chemotherapy.

Auto-fluorescence measurements and data analysis

For AF intensity measurements, four instruments were used corresponding to each excitation wavelength. For 365 nm excitation, the light from a 365 nm high power LED (190 mW, Thorlabs) was focused on the sample *via* a collimating lens and a 2× infinity corrected objective at an approximately 45° angle. The AF light was collected with another 2x microscope objective mounted on a microscope. The AF light was filtered with a 400-800 nm band pass filter and then coupled to a spectrometer (150 lines/mm grating and DU 401 series CCD, Andor, UK) using a multimode optical fibre. The same microscope was also used for the acquisition of AF spectra for 671 nm excitation, using a CW laser with maximum power of 250 mW (Gem 671, LaserQuantum, USA) and a grating of 600 lines/mm. For the 775 nm excitation, a Nikon Eclipse inverted microscope equipped with a 20x objective connected to a pulsed laser (Katana 775, OneFive, 775 nm, 50 mW average power, 30 ps pulse width at 10 MHz repetition rate) and connected using a multimod fibre to a spectrometer (600 lines/mm grating and DU401 CCD, Oxford Instruments).

The statistical significance of differences observed in the intensity of AF spectra of normal and CRLMs was determined using a two-sample *t*-test. The spectra consisted of 1024 intensity values corresponding to 1024 different wavelengths (as recorded on the instrument CCD). The MATLAB function (ttest2) was used to calculate the *P* values resulting in 1024 values. The maximum and the mean of the 1024 *P* values were used to determine statistical difference.

Raman spectroscopy and data analysis

The operating mechanism of the Raman instrument (RiverD International) has previously been described.[10] The instrument was equipped with a CW 785 nm laser for excitation (~70 mW power) and spectrometer with an iVAC CCD (Oxford Instruments). For each tissue specimen, approximately 100 spectra were measured (acquisition time of 2 s/spectrum). Spectra corresponding to surgical ink and spectra with a low signal to noise ratio were removed from the spectral dataset. Surgical ink was identified by the presence of sharp Raman bands at 680 cm^{-1} and 746 cm^{-1}. Spectra were considered to have low signal if the ratio between the intensity of the 1450 cm^{-1} band and the variance of noise was lower than 10. The mean spectrum and standard deviation were then computed for each tissue specimen.

Results

Auto-fluorescence spectroscopy

AF emission spectra were collected using different excitation wavelengths to determine the optimal excitation conditions that provide highest contrast between normal liver tissue and CRLM. The average AF emission intensity spectra collected using excitation wavelengths at 365 nm, 671 nm, and 785 nm in both normal liver tissue and CRLM are shown in Figure 1.

Figure 1A showed that on average an approximately three-fold higher AF intensity for CRLM compared to normal liver tissue was observed when 365 nm was used for excitation. Emission spectra with a 365-nm excitation were recorded from the healthy and cancerous regions of specimens obtained from four patients. The AF intensity spectra showed a large variance and overlapped with the spectra of normal liver tissue. A two-sample *t*-test was conducted for each wavelength from the AF spectrum and the resulting *P* values were averaged, producing a mean *P* value of 0.18 (*P* value distribution for each wavenumber is shown in Fig. S3), suggesting that the difference is not statistically significant.

The largest contrast in AF intensity between CRLM and normal liver tissue was observed when 671 nm and 775 nm excitation wavelengths were applied, as seen in Figure 1B and C. For both wavelengths, the AF intensity from normal liver

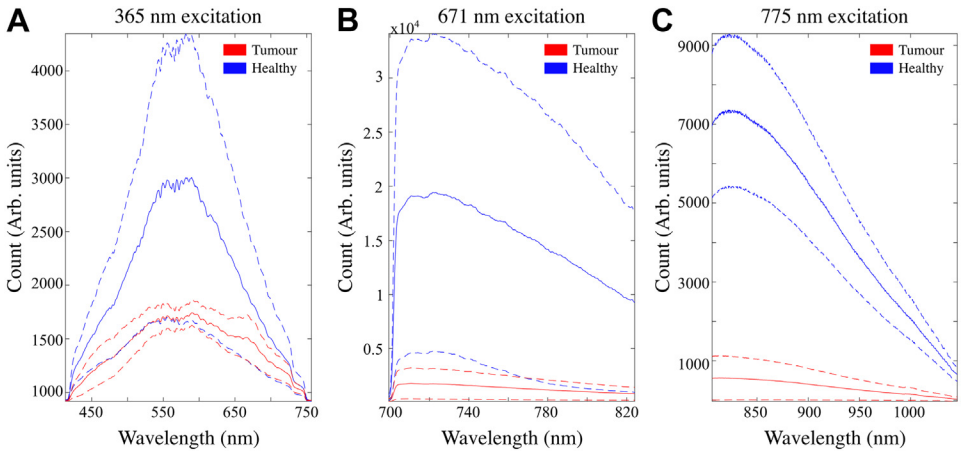

Fig. 1 – AF emission spectra of normal liver tissue and colorectal liver metastases (CRLMs) measured at different excitation wavelengths: (A) 365 nm high-power LED; (B) 671 nm laser; and (C) 785 nm laser. Continues lines represent averages from multiple patients: (A) four patients, (B) 12 patients, and (C) five patients. The dotted line represent ± standard deviations.

tissue was around eight-folds higher than for CRLM, with significantly less overlap. The resulting mean *P* values following the two-sample t-test produced a mean *P* value of 0.00045 for the 671 nm excitation (spectra from 12 patients) and a mean *P* value of 0.000057 for the 775 nm excitation (spectra from five patients). For these two excitations, the difference observed between the two tissue types was shown to be of relevant significance.

Overall, these results suggest that applying the wavelength excitation at 671 nm or 785 nm provides a significant advantage compared to the 365 nm wavelength. These benefits were observed with respect to signal intensity and improved contrast between normal liver tissue and CRLMs, and hence were selected for further investigation.

Near-infrared auto-fluorescence mapping

AF intensity mapping was used to determine the variance of AF signals caused by molecular heterogeneity of normal liver tissue and CRLM. Typical AF intensity maps of a tissue sample from the same patient measured by both 671 nm and 785 nm excitation are shown in Figure 2. A two-sample *t*-test was conducted for each wavelength from the AF spectra for a random sampling of 100 spectra from all raster-scanned tissue specimens. The largest *P* value observed in the AF maps obtained at 671 nm excitation was 0.000066 (mean value of 1.7×10^{-9}) and the largest *P* value observed for the 775 nm excitation was 0.0167 with a mean value of 1.09×10^{-5}. These results confirm that overall normal liver

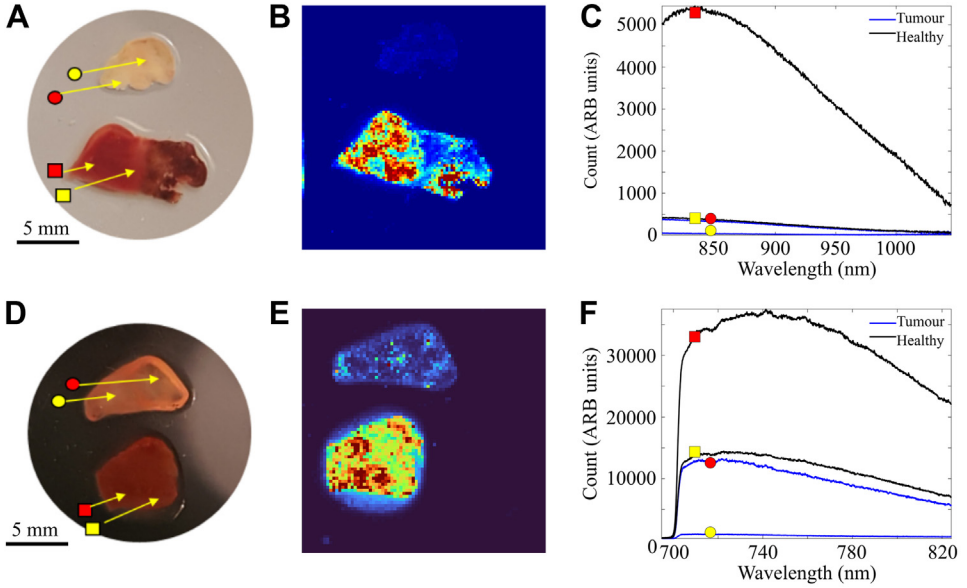

Fig. 2 – AF intensity mapping of typical normal liver tissue and CRLMs using near-infrared excitation wavelengths. (A and D) brightfield images (square symbols: normal liver, circle symbols: CRLMs). AF maps corresponding to 775 nm (B) and 671 nm excitation (D). Images 100 × 100 pixels, step size: 100 μm, dwell time: 0.2 s/pixel. AF spectra at location selected in (A) and (D) are presented in for 775 nm (C) and 671 nm (F) excitation, respectively.

tissue had a significantly higher AF intensity compared to CRLMs.

The results also show that AF intensity of normal liver tissue can vary across the tissue sample because of tissue heterogeneity.

The maps in Figure 2B and E show that certain parts of normal liver tissue can have low AF intensity as seen in CRLMs. The emission spectra from regions of normal liver tissue with low AF intensity are comparable to the emission spectra from regions of tumour with high AF intensity, suggesting potential overlap of the AF intensity between the tissue types. This could potentially decrease the specificity of AF intensity, as regions of normal liver tissue may be incorrectly classified as CRLMs.

Following this observation, the consistency of AF mapping was compared using samples from 12 patients. There were three samples that were not used as these samples were insufficient following the initial experiment. The AF maps in Figure 3 were presented using the same intensity scale and confirmed the consistency of the 775 nm induced AF intensity for discriminating between normal liver tissue and CRLMs but highlighted also that most normal liver specimens had small regions with low AF that could potentially be misclassified as CRLM. However, in the tumour specimen of Sample 2, the AF signal is unusually high. On histology analysis, this sample showed complete response to chemotherapy with no residual tumour detected. However, surgical resection was based on liver metastases demonstrated on radiological imaging which included computed tomography and magnetic resonance imaging. While Sample 2 showed large areas of normal liver tissue with "low AF intensity", smaller regions can also be identified in Sample 6, 8, 9, and 13 (red arrows).

While the results in Figures 1 and 3 show that AF intensity based on 671 nm and 785 nm excitation is significantly different for CRLM compared to normal tissue ($P < 0.0167$), the presence of normal tissue with low AF intensity may lead to false-positive detections. Therefore, we investigate whether Raman spectroscopy could be used as an additional technique to identify differences between CRLM and normal tissue with low AF intensity.

Raman spectroscopy

Because excitation at 365 nm was performed with an LED (broad spectrum), Raman spectra were collected only for laser excitation at 671 nm and 785 nm. However, Raman bands were detected above the AF background only when using the 785 nm laser (Supplementary Information Fig. S4).

A representative example of normal liver tissue and CRLM from the same patient, with the normal tissue having a region

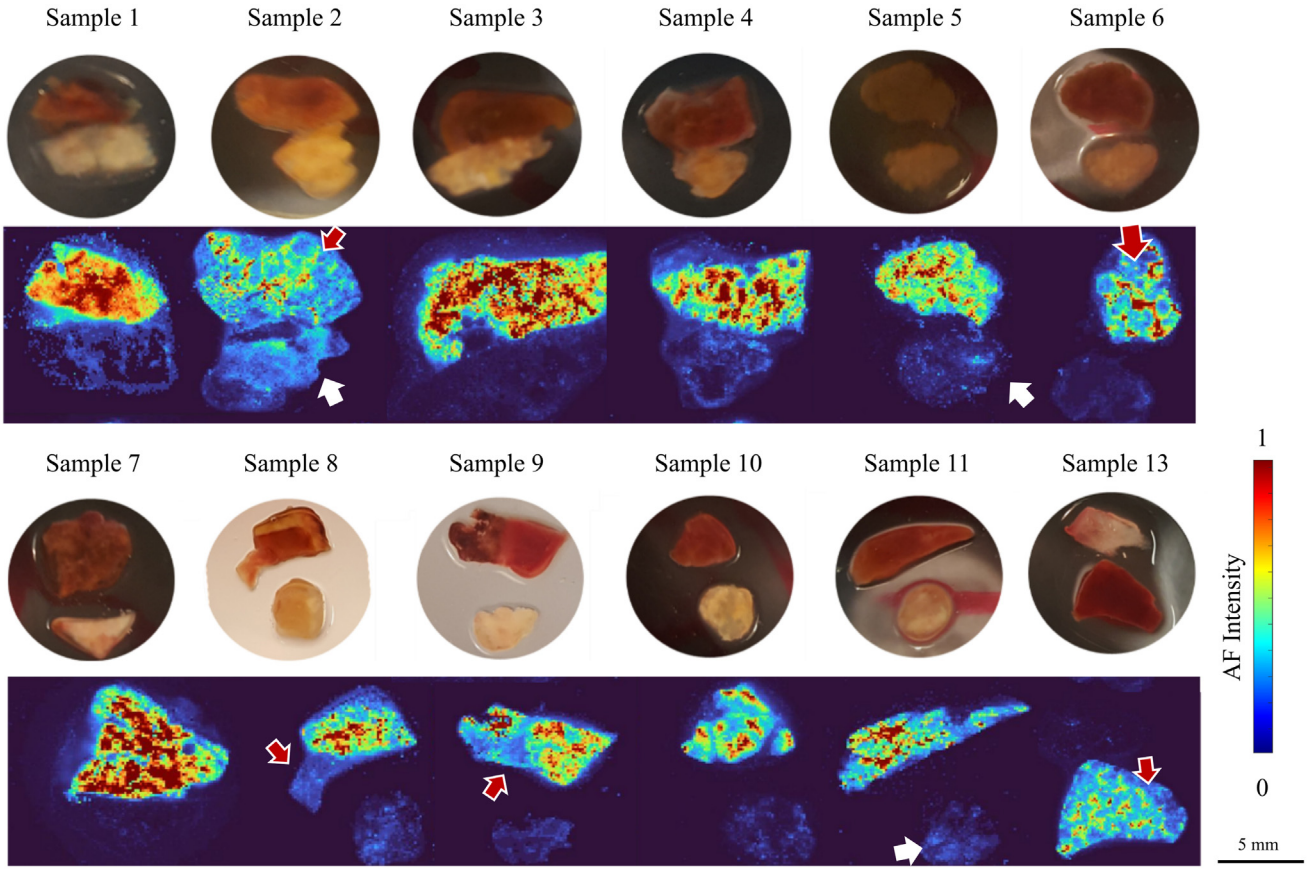

Fig. 3 – Brightfield images and 775 nm excited AF mapping of normal liver tissue and CRLMs for surgical specimens from 12 patients. The intensity scale was normalized to unity based on AF intensity from all samples. Scale bars apply to all AF images. Red arrows indicate regions of "low AF intensity" in normal liver tissue and white arrows indicate regions of "high AF intensity" for CRLM.

of "low AF intensity" is demonstrated in Figure 4A and B. Figure 4C shows that the emission spectrum from the "high AF intensity" regions of the normal liver tissue (marked by a yellow circle) is dominated by fluorescence emission and no Raman bands were identified. Figure 4D compares the spectra from CRLM (point with high AF intensity, as shown in Fig. 4B) and "low AF intensity" region of the normal liver tissue. While the spectrum of "high AF intensity" CRLM (marked by red square) has a substantial fluorescence background, clear Raman bands were identified, which can be assigned to the main biomolecules in liver tissue such as proteins, nucleic acids, lipids, and carbohydrates. On the other hand, the spectrum measured from the "low AF intensity" region of normal liver tissue (marked by yellow square) has a higher fluorescence background and almost no Raman bands can be identified. These results suggest that Raman spectroscopy could be used to discriminate between "low AF intensity" regions of normal liver tissue and "high AF intensity" observed in CRLM.

Following the above findings, Raman bands were investigated to determine whether the spectra recorded from CRLM specimens from different patients can be related to dominant tissue types.

Three distinct types of Raman spectra were typically observed in the 12 tissue specimens containing CRLM (Fig. 5). While all spectra contained bands characteristic to cells and tissue, for five of the 12 tissue specimens investigated in this part (samples 9, 10, 11, 13, 14, 15), the mean spectrum showed higher contribution from bands assigned to DNA (Fig. 5A):

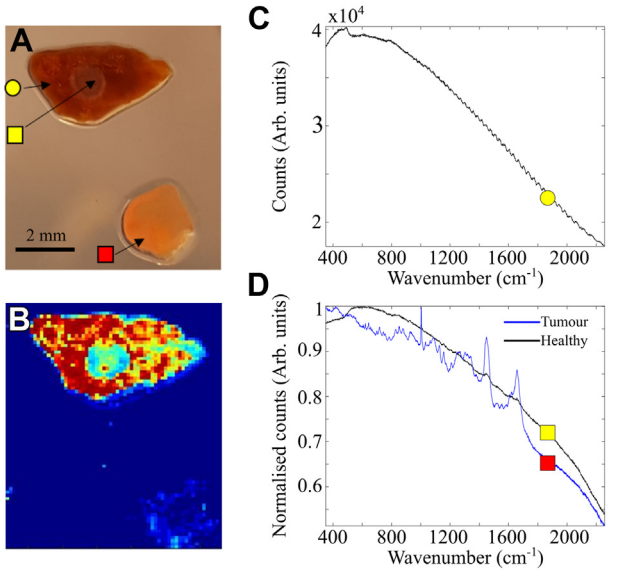

Fig. 4 – Comparison between Raman spectra of normal liver tissue and CRLM sing 785 nm laser excitation (Sample 13). (A) Brightfield images, yellow marks (circle and square) represent normal tissue, and red square represents CRLM. (B) AF mapping (785 nm excitation). (C) Typical AF/Raman spectrum corresponding to normal liver tissue (yellow circle). (D) Comparison between AF/Raman spectra from "high AF intensity" CRLM position [red square in (A)] and "low AF intensity" normal liver [yellow square in (A)].

788 cm^{-1} band corresponds to the symmetric stretching of O-P-O, the 1098 cm^{-1} band to PO_2^- stretching. These results agreed with the histology sections which showed a large number of tumour cells with increased nucleic-to-cytoplasm ratio or large areas of necrosis.

Raman spectra with strong contributions from collagen, such as bands represented by the bands at 857 cm^{-1}, 938 cm^{-1}, and 1250 cm^{-1} (Fig. 5B), were identified in samples 1, 2, 3, 7, 8, 9, 11, 15. These bands were correlated with areas of fibrosis and hylane matrix in the CRLM, as observed in the hematoxylin and eosin staining example in Figure 5B. Some spectra from sample 2, which had no visible tumour following chemotherapy, defined as complete response, also indicated intense bands assigned to collagen and confirmed by histology, which showed a high level of fibrous histiocytomas, which are benign neoplasms composed of fibroblastic and histiocytic cells and scattered inflammatory cells (Fig. 5B).

Spectra with strong contribution from lipids (Fig. 5C) were also identified, in particular in samples 8 and 15. Histology indicated that these spectra can be assigned to steatosis, which was detected in these samples. These results agree with previous reports on mouse liver steatosis, indicating Raman bands assigned to cholesteryl esters, such as C=C stretch band at 1660 cm^{-1}, CH_2 and CH_3 bend bands at 1450 cm^{-1}, and the CH_2 and =CH bend band at 1260 cm^{-1} (Fig. 5C).

These results show that Raman spectroscopy using 785-nm excitation cannot be used to discriminate between normal liver tissue and CRLM because of the inability to detect Raman bands from normal tissue. Nevertheless, the Raman spectra measured from CRLM specimens denote the presence of tissue structures that are present in metastatic liver tissue, such as pleomorphic malignant cells, fibrotic tissue, and cholesterol clefts. As such, this technique shows that a "low AF intensity" region for which the Raman bands are detectable and match the patterns showed in Figure 5 is likely corresponds to CRLM.

Auto-fluorescence–Raman analysis of mixed colorectal liver metastases and normal tissue

The next stage of the project was to assess whether a dual-modality approach based on AF-Raman spectroscopy could be suitable for intraoperative detection of CRLMs in *ex vivo* resected liver specimens. AF intensity imaging based on 785 nm excitation was used for fast mapping of the tissue specimens and any regions of low AF intensity could be further analyzed by Raman spectroscopy point measurements (using the same laser) to confirm whether these regions are normal liver tissue or CRLM. This approach was tested using a constructed liver sample in which small pieces of CRLM tissue (typically 1-2.5 mm in size, approximately 0.5 mm thickness) were placed on a quartz window and covered with a large sample of normal liver tissue (approximately 15 mm in size, 5-6 mm thickness) to potentially mimic a real resection liver specimen of CRLM with positive margins. Although this was not a true sample, the aim of this experiment was to assess the combined AF-Raman technique on a liver resection specimen of CRLM with positive margins.

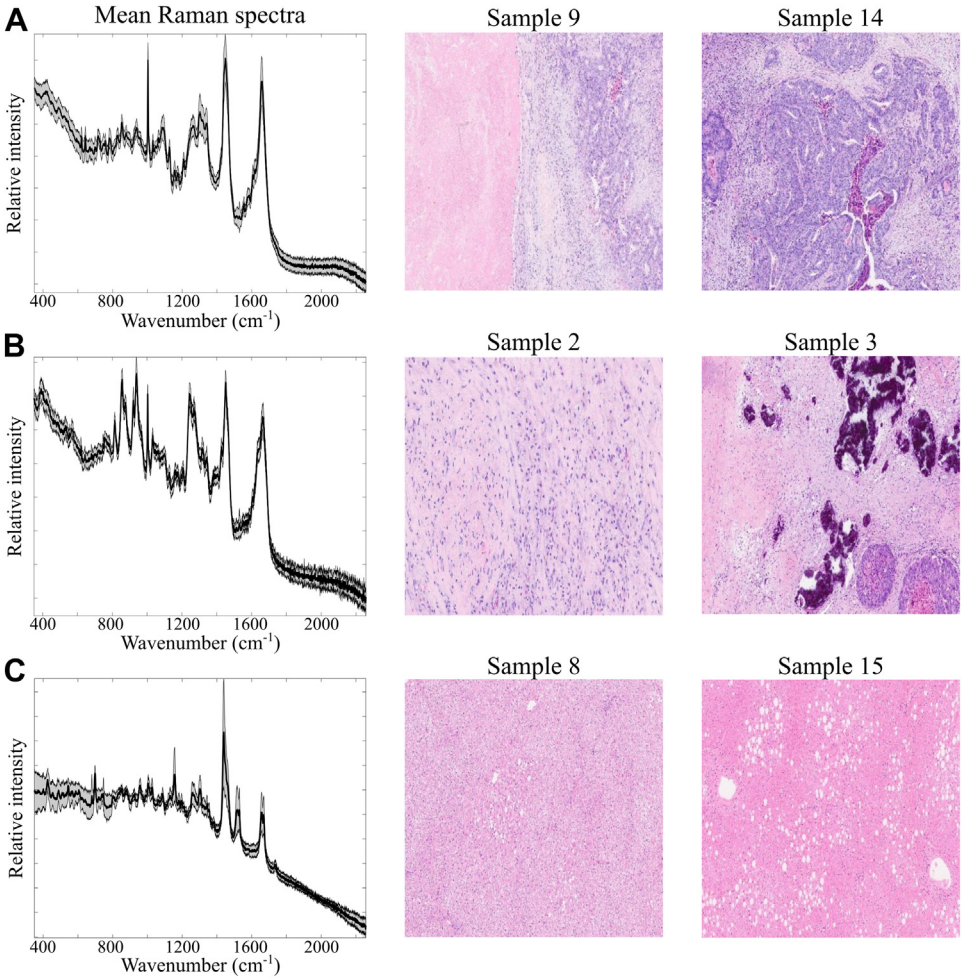

Fig. 5 – Typical Raman spectra of CRLM (785 nm laser). Three main types of spectra were observed: (A) Tissue containing higher proportion of malignant cells (high nucleus/cytoplasm ratio) (Sample 14) and/or necrosis (Sample 9). (B) Tissue containing a high concentration of collagen, such as abundant fibrohistiocytic reaction (Sample 2) or hyaline changes and calcification (Sample 3). (C) Tissue containing high lipid content related to steatosis (grade 1 in Sample 8, grade 3 in Sample 15). The spectra represent the average spectrum from a tissue specimen and the per specimen standard deviation as a grey shadow.

Figure 6A shows a brightfield image of the tissue surface subjected to AF-Raman measurements, with black arrows indicating the small CRLM regions. Figure 6B shows the 775 nm excited AF image of the sample, which demonstrates that all seven CRLMs specimens were detected as having low AF intensity. The sample was moved on the Raman microscope (785 nm laser) and a raster map was recorded from the highlighted region that contained one CRLM region. The raster Raman map (Fig. 6C) confirms that the surrounding normal tissue had higher AF intensity compared to the CRLM region. Figure 6D presents three typical Raman spectra from three locations within the low AF intensity region, confirming that the Raman spectra are similar to the previously measured spectra of CRLM, displaying spectral features specific to DNA and collagen (Fig. 5A and B). Although the CRLM fragments were as thin as 0.5 mm, the confocal set up of the Raman microscope successfully suppressed the AF photons from the bulk of normal liver tissue. It is worth noting that the raster Raman scan was included here to confirm the repositioning of the sample after transfer from the AF microscopes. Raster scanning Raman spectroscopy would not be required for an integrated AF-Raman instrument.

For the sample in Figure 6B, the measurement time for AF map (excluding the Raman raster scan) was 66 min in total: approximately 33 min for data acquisition (100 × 100 pixels, at 0.2 s/pixel dwell time, step size 200 μm) and approximately 33 min for data transfer and translation stage required for sample scanning. The identification of the CRLM regions can be confirmed with 3-5 Raman spectra per region, requiring approximately 1 min for all seven regions (integration time 2 s/spectrum).

Discussion

Colorectal cancer is a leading cause of cancer-associated death in Western populations and around 25%-30% of patients diagnosed with colorectal cancer develop liver

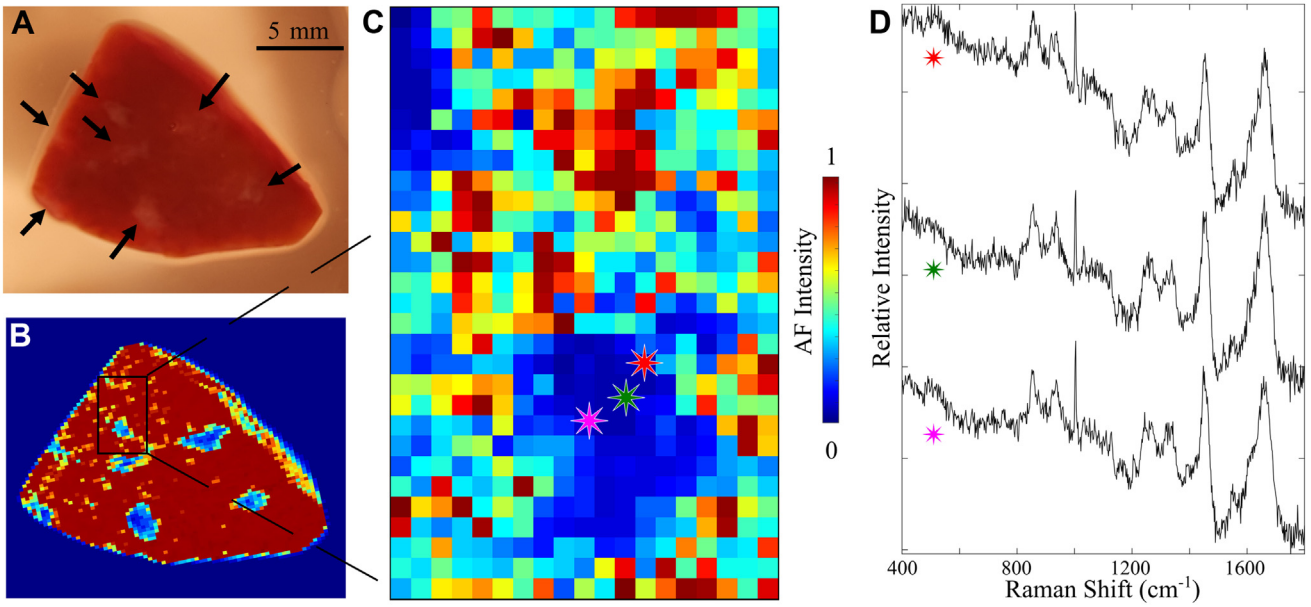

Fig. 6 – AF mapping and Raman spectroscopy of a mixed sample consisting of CRLM tissue (~0.5 mm thick) covered by bulk normal liver tissue. (A) Brightfield images of the sample, black arrows indicate the CRLM regions. (B) AF intensity map at 785 nm excitation; (C) Detail AF map of the selected region in (B) that includes CRLM; (D) Raman spectra at selected points in (C). Excitation 785 nm, 2 s/pixel integration time.

metastases during the course of their disease.[1,2] Resection rates and oncological outcome have increasingly improved in recent years due to advances in surgical techniques, preoperative imaging, perioperative management, and systemic therapy. In cases of heavy disease burden, parenchymal-sparing liver resection has allowed for an increase in resection rates. In these cases, there is a potential for higher R1 resection rates. R1 resection has been associated with poorer survival outcomes and developing an intraoperative technique that enables surgeons to have a clear margin during surgery could potentially improve outcomes.[23]

With respect to AF spectra of liver tissue, this study observed that 671 nm and 785 nm excited AF spectra can be used to discriminate CRLM from normal liver tissue with high sensitivity. When other excitation wavelengths were used, such as the 365 nm, the AF intensity spectra showed a large variance and overlapped with the spectra of normal liver tissue. These findings agree with previous reports based on 377 nm excitation, which assigned the AF spectra to collagen, elastin, NADH, and FAD but found that only the ratio NADH/(NADH + FAD) values were significantly different (collagen and elastin signals were not statistically different).[24] In addition, the AF spectra contained signals from fluorophores in tissue; the bands at 650 nm can be assigned to porphyrins.[25] Although the origin of the fluorophore was not confirmed, previous reports indicated intense AF emission above 800 nm from bilirubin (including bilirubin in liver) can be excited in a broad range of wavelengths in the 600-785 nm range.[26] Analysis of the AF emission peaks at 635 nm and 670 nm enabled distinction of benign liver lesions from potentially evolutive liver nodules with a high sensitivity and specificity of 78% and 91%, respectively. AF imaging has also been applied for *in vivo* identification of CRLM during surgery, in conjunction with diffuse reflectance spectroscopy.[24] Based on samples from 19 patients, AF intensity induced by a 377-nm laser coupled to needle-probe provided a sensitivity and specificity of 84% and 61%, respectively, in differentiating CRLMs from normal liver tissue.[24]

Recent work by other groups showed that 785 nm excitation can also be used for intraoperative localization of the parathyroid glands in patients undergoing surgery for parathyroid and thyroid gland disease[27,28] and for identification of atherosclerotic plaques with intraplaque hemorrhage.[26] Using animal models, these studies showed that the near-infrared AF was associated with the presence of intraplaque hemorrhage and hem degradation products, particularly bilirubin.[26] Thus, it is likely that the high contrast in the AF intensity between normal liver and CRLM found in this study relies on lower concentration of bilirubin in CRLM compared to normal liver tissue. Of note, patients with CRLM who undergo liver resection have a bilirubin at normal range as their pathology does not present with obstructive jaundice and these patients have a normal liver parenchymal, unlike patients with hepatocellular carcinoma that tend to arise from a background of liver cirrhosis and may have liver dysfunction.

With the introduction of Raman spectroscopy, only excitation with 785 nm laser allowed detection of Raman bands above the AF level. However, the spectrum of high AF intensity in CRLM tissue has a significant fluorescence background, which can be assigned to the main biomolecules in tissue (proteins, nucleic acids, lipids, and carbohydrates).[9] In addition, the Raman spectra observations with respect to the presence of malignant cells are consistent with previous Raman spectra reported for tumours from other tissue types, such as skin[29,30] or breast.[31] Although the 785-nm induced AF intensity could lead to false-positive detections because some

regions of normal liver tissue can also have lower AF intensity, the addition of Raman spectroscopy (using the same 785 nm laser) could be used to confirm the presence of CRLM and provide the required specificity needed for clinical applications. Pence *et al.* previously demonstrated that 1064 nm laser excitation and dispersive spectrographs with InGaAs detectors significantly reduced AF and allowed discrimination between normal and liver tumours, albeit long integration times (30 s per spectrum) are required.[32] It must be noted that in this study it is likely that these two techniques are able to differentiate normal liver tissues and abnormal tissue in this case CRLM. Further studies are needed to establish spectral difference between normal and cancer cells, to discriminate between malignant tumour and benign neoplasms.

Although Raman spectroscopy is much slower and typically impractical for intraoperative tissue imaging, it may be used to record only a reduced number of measurements to discriminate between "low AF intensity" normal liver and "high AF intensity" CRLM. However, the combination of AF and Raman spectroscopy could be used to achieve both high sensitivity and high specificity, without significantly increasing the measurement time. Previous studies showed that AF-Raman techniques can be integrated in a single device suitable to use in a clinical environment to scan *ex vivo* surgical skin specimens during Mohs micrographic surgery.[11,12] In addition, compared to the fresh frozen technique, the AF-Raman technique would require no tissue sectioning or staining and no urgent requirement of histopathologic input as this technique would provide an objective diagnostic map showing the location of tumour. The standard identification of tumour cells on the liver samples with this technique will also minimize subjectivity and increase reporting efficiency.

Both AF and Raman spectra are specific to the endogenous molecules in tissue. Discriminations between normal tissue and cancer rely on molecular differences that are either the cause or the effect of disease. Therefore, these spectra are highly specific to the organ itself. While AF and Raman spectroscopy can be considered platform technologies, the instrument would require fine-tuning of the excitation wavelengths and detected Raman bands to take into consideration organ-specific molecules.

The focus of this proof-of-concept study was to identify the conditions for optimizing contrast between CRLM and normal liver tissue, not necessarily minimizing acquisition time. For the instruments used in this study, the imaging speed was limited by the CCD (minimum dwell time 0.2 s/spectrum) and the translation stage used for sample scanning (approximately 0.2 per step), not the photon count. The imaging speed could be significantly improved with a higher speed NIR CCD (same quantum efficiency $>$ 80%) allowing dwell times of approximately 500 μs. At this dwell time, it is estimated on average 5×10^3 counts for CRLM samples and 75×10^3 counts for normal liver tissue samples. The translation stage could be replaced by galvo-scanners to reduce the time lost for stage sample scanner. Under these conditions, imaging a 2×2 cm^2 tissue area would require an estimated time of 10-15 s, at a resolution of 200 μm. From this study, it is unclear how many "low AF intensity" regions a normal liver tissue would have to estimate the number of spectra required. However, the acquisition time for Raman spectra was 2 s/spectrum; therefore, 30 spectra could be acquired within 1 min. Higher number of Raman spectra can also be recorded simultaneously by using multifoci Raman spectroscopy, as demonstrated previously in conjunction with AF imaging for detection of nonmelanoma skin cancers.[33] These calculations indicate the potential of using the combined AF-Raman technique for *ex vivo* detection of surgical margins with tumour involvement. While previous studies have demonstrated that exogenous molecules (e.g., fluorescein, indocyanine green, fluorescent antibodies) can improve the contrast between normal liver tissue and malignant tissue,[34-36] these techniques require the administration of the contrast agents up to several days prior to surgery. This significant drawback is eliminated by the AF-Raman approach because it targets endogenous molecules to detect the presence of CRLM.

There are a few limitations in this study. As this was a proof-of-concept study, the small number of patients recruited precludes the use of statistical analysis to determine any significant effect. The study was conducted on tissue samples obtained from colorectal liver metastases; hence, these samples had either a normal background liver in patients who did not receive preoperative chemotherapy or steatosis and/or sinusoidal obstruction syndrome features in the background liver which are consistent with chemotherapy changes. Therefore, this study was unable to determine the impact of fibrosis and/or cirrhosis with respect to differentiating the background liver tissue with these features and liver tumours. The current technique has been tested in the laboratory setting and the next stage of the project is to investigate the utility of this technique on other liver tumour types such as hepatocellular carcinoma which is associated with cirrhosis and fibrosis, and also, attempt to replicate this technology in a clinical setting.

This study reports the first use of near-infrared AF imaging and Raman spectroscopy for discriminating CRLM from normal liver tissue in an *ex vivo* setting. The results showed that AF excitation at 671 nm and 775/785 nm wavelengths provided a high level of tissue contrast. Although the instrument used here required long imaging time, optimization of the detectors and use of galvo-scanners could achieve quicker analysis. The integration of Raman spectroscopy using 785-nm laser was used for recording Raman spectra from parts of normal tissue that elicited low AF intensity to discriminate such regions from CRLM. These results demonstrate the potential of AF-Raman spectroscopy for intraoperative *ex vivo* detection of CRLM.

Conclusions

AF imaging and Raman spectroscopy are able to discriminate CRLM from normal liver tissue in an *ex vivo* setting. This laboratory concept that exploits the main advantages of these two complementary techniques and potentially could provide a practical solution to increase diagnosis accuracy and imaging speed. This is the first step to explore the potential of this technology for future intraoperative use in liver surgery. Further studies are required to develop an optimized integrated AF-Raman device that could be tested on a large number of patients to determine its accuracy in a clinical setting.

Supplementary Materials

Supplementary data related to this article can be found at https://doi.org/10.1016/j.jss.2023.02.014.

Author Contributions

C.C., R.B., P.S.D., and A.H. collected samples and conducted experiments; A.M., D.G., and I.N. designed and supervised the research and wrote the paper.

Acknowledgments

This work was supported by the UK Medical Research Council [grant number MC_PC_18058]. We acknowledge the help of Dr Kevin Hughes for useful discussions.

Disclosure

I. Notingher holds a patent related to the multimodal imaging based on AF and Raman spectroscopy.

Funding

This work was supported by the UK Medical Research Council [grant number MC_PC_18058].

REFERENCES

1. Adam R, De Gramont A, Figueras J, et al. The oncosurgery approach to managing liver metastases from colorectal cancer: a multidisciplinary international consensus. *Oncologist*. 2012;17:1225–1239.
2. Manfredi S, Lepage C, Hatem C, et al. Epidemiology and management of liver metastases from colorectal cancer. *Ann Surg*. 2006;244:254–259.
3. Creasy JM, Sadot E, Koerkamp BG, et al. Actual 10-year survival after hepatic resection of colorectal liver metastases: what factors preclude cure? *Surgery*. 2018;163:1238–1244.
4. Kanas GP, Taylor A, Primrose JN, et al. Survival after liver resection in metastatic colorectal cancer: review and meta-analysis of prognostic factors. *Clin Epidemiol*. 2012;4:283–301.
5. Margonis GA, Sergentanis TN, Ntanasis-Stathopoulos I, et al. Impact of surgical margin width on recurrence and overall survival following R0 hepatic resection of colorectal metastases: a systematic review and meta-analysis. *Ann Surg*. 2018;267:1047–1055.
6. Siebenhüner AR, Güller U, Warschkow R. Population-based SEER analysis of survival in colorectal cancer patients with or without resection of lung and liver metastases. *BMC Cancer*. 2020;20:246.
7. Voskuil FJ, Vonk J, van der Vegt B, et al. Intraoperative imaging in pathology-assisted surgery. *Nat Biomed Eng*. 2021;6:503–514.
8. Stewart HL, Birch DJS. Fluorescence guided surgery. *Methods Appl Fluoresc*. 2001;9:42002.
9. Shipp DW, Sinjab F, Notingher I. Raman spectroscopy: techniques and applications in the life sciences. *Adv Opt Photon*. 2017;9:315–428.
10. Kong K, Rowlands CJ, Varma S, et al. Diagnosis of tumors during tissue-conserving surgery with integrated autofluorescence and Raman scattering microscopy. *Proc Natl Acad Sci U S A*. 2013;110:15189–15194.
11. Boitor R, Kong K, Shipp D, et al. Automated multimodal spectral histopathology for quantitative diagnosis of residual tumour during basal cell carcinoma surgery. *Biomed Opt Express*. 2017;8:5749–5766.
12. Boitor R, de Wolf C, Weesie F, et al. Clinical integration of fast Raman spectroscopy for Mohs micrographic surgery of basal cell carcinoma. *Biomed Opt Express*. 2021;12:2015–2026.
13. Kong K, Zaabar F, Rakha E, et al. Towards intra-operative diagnosis of tumours during breast conserving surgery by selective-sampling Raman micro-spectroscopy. *Phys Med Biol*. 2014;59:6141–6152.
14. Shipp DW, Rakha EA, Koloydenko AA, et al. Intra-operative spectroscopic assessment of surgical margins during breast conserving surgery. *Breast Cancer Res*. 2018;20:69.
15. Croce AC, Ferrigno A, Bottiroli G, et al. Autofluorescence-based optical biopsy: an effective diagnostic tool in hepatology. *Liver Int*. 2018;38:1160–1174.
16. Maki H, Kawaguchi Y, Arita J, et al. Real-time confocal laser endomicroscopic evaluation of primary liver cancer based on human liver autofluorescence. *J Surg Oncol*. 2017;115:151–157.
17. Jermyn M, Desroches J, Aubertin K, et al. Raman spectroscopy advances with an emphasis on clinical translation challenges in oncology. *Phys Med Biol*. 2016;61:R370–R400.
18. Santos IP, Barroso EM, Bakker Schut TC, et al. Raman spectroscopy for cancer detection and cancer surgery guidance: translation to the clinics. *Analyst*. 2017;142:3025–3047.
19. Hubbard TJE, Shore A, Stone N. Raman spectroscopy for rapid intra-operative margin analysis of surgically excised tumour specimens. *Analyst*. 2019;144:6479–6496.
20. Lizio MG, Boitor R, Notingher I. Selective-sampling Raman imaging techniques for ex vivo assessment of surgical margins in cancer surgery. *Analyst*. 2021;146:3799–3809.
21. Huang N, Short M, Zhao J, et al. Full range characterization of the Raman spectra of organs in a murine model. *Opt Express*. 2011;19:22892–22909.
22. Corden C, Boitor R, Notingher I. Time-gated Raman spectroscopy for biomedical application under ambient or strong background light conditions. *J Phys D Appl Phys*. 2021;54:504003.
23. Viganò L, Costa G, Cimino MM, et al. R1 resection for colorectal liver metastases: a survey questioning surgeons about its incidence, clinical impact, and management. *J Gastrointest Surg*. 2018;22:1752–1763.
24. Tanis E, Evers DJ, Spliethoff JW, et al. In vivo tumor identification of colorectal liver metastases with diffuse reflectance and fluorescence spectroscopy. *Lasers Surg Med*. 2016;48:820–827.
25. Benoit C, Rodrigues A, Calderaro J, et al. Autofluorescence imaging within the liver: a promising tool for the detection and characterization of primary liver tumors. *Eur Radiol*. 2022;32:2481–2491.
26. Htun NM, Chen YC, Lim B, et al. Near-infrared autofluorescence induced by intraplaque hemorrhage and heme degradation as marker for high-risk atherosclerotic plaques. *Nat Commun*. 2017;8:75.
27. McWade MA, Paras C, White LM, et al. Label-free intraoperative parathyroid localization with near-infrared autofluorescence imaging. *J Clin Endocrinol Metab*. 2014;99:4574–4580.

28. Mannoh EA, Parker LB, Thomas G, et al. Development of an imaging device for label-free parathyroid gland identification and vascularity assessment. *J Biophot*. 2021;14:e202100008.
29. Nijssen A, Maquelin K, Santos LF, et al. Discriminating basal cell carcinoma from perilesional skin using high wave-number Raman spectroscopy. *J Biomed Opt*. 2007;12:34004.
30. Larraona-Puy M, Ghita A, Zoladek A, et al. Development of Raman microspectroscopy for automated detection and imaging of basal cell carcinoma. *J Biomed Opt*. 2009;14:54031.
31. Haka AS, Shafer-Peltier KE, Fitzmaurice M, et al. Diagnosing breast cancer by using Raman spectroscopy. *Proc Natl Acad Sci U S A*. 2005;102:12371–12376.
32. Pence IJ, Patil CA, Lieber CA, et al. Discrimination of liver malignancies with 1064 nm dispersive Raman spectroscopy. *Biomed Opt Express*. 2015;6:2724–2737.
33. Sinjab F, Kong K, Gibson G, et al. Tissue diagnosis using power-sharing multifocal Raman micro-spectroscopy and auto-fluorescence imaging. *Biomed Opt Express*. 2016;7:2993–3006.
34. Goetz M, Deris I, Vieth M, et al. Near-infrared confocal imagingduring mini-laparoscopy: a novel rigid endomicroscope withincreased imaging plane depth. *J Hepatol*. 2010;53:84–90.
35. Hiroshima Y, Lwin TM, Murakami T, et al. Effective fluorescence-guided surgery of liver metastasis using a fluorescent anti-CEA antibody. *Surg Oncol*. 2016;114:951–958.
36. Schneider C, Johnson SP, Gurusamy K, et al. Identification of liver metastases with probe-based confocal laser endomicroscopy at two excitation wavelengths. *Lasers Surg Med*. 2017;49:280–292.